Adsorption Behavior of Rifampicin from Aqueous Solution onto Locally Available Mud: Equilibrium, Kinetics, and Thermodynamic Study

Altamer, Duaa H.
Department of New and Renewable Energies, College of Science, Mosul University, Mosul, IRAQ

Alqazzaz, Wael A.; Fadhi, Abdelrahman B.*[+]
Department of Chemistry, College of Science, Mosul University, Mosul, IRAQ

ABSTRACT: *Several methods have been implemented to eliminate antibiotics from wastewater. Serious issues are associated with the disposal of antibiotics into the aqua resources, resulting in the contamination of these systems. The utilization of natural adsorbents, like clays and naturally derived adsorbents, have been tried to solve this problem. Red mud was examined as an adsorbent for multiple pollutants in this regard. This work reports the utilization of the Iraqi red mud as a priceless and effective adsorbent for eliminating the Rifampicin antibiotic from its aqueous solution after being activated with 10 % HCl to enhance its surface area. BET surface area, Field Emission Scanning Electron Microscope, Fourier Infra-Red spectroscopy, Energy Dispersive X-ray, and X-ray Diffraction of both the raw mud and its activated sample were determined. The BET surface area of the Iraqi red mud raised from 30.99 m^2/g to 60.96 m^2/g because of the acid treatment. The influence of the adsorption operative factors, including the solution pH, Rifampicin initial concentration, adsorbent dosage, temperature, and contact time, on Rifampicin elimination by the activated red mud, was inspected. The typical adsorption capacity of Rifampicin by the activated red mud was 217.93 mg/g utilizing 0.20 g of the activated red mud at 328 K for 180 minutes contact time in an acidic medium (pH = 4.0). The Langmuir model best described the adsorption behavior of Rifampicin over the activated red mud due to its higher correlation coefficient value (R^2 = 0.9928) than that of the Freundlich model (R^2 = 0.9117). Rifampicin adsorption by the activated red mud followed the pseudo-second-order kinetic model. Thermodynamic analysis revealed that the adsorption of Rifampicin favored high temperatures, suggesting that the adsorption is endothermic in nature and spontaneous. Finally, the activated red mud is an eco-friendly and reusable adsorbent to remove antibiotic pollutants.*

KEYWORDS: *Acid-treated Red Mud; Activated Red Mud; Rifampicin antibiotic; Adsorption isotherms and kinetics; Adsorption mechanism; Reusability*.

***** *To whom correspondence should be addressed.*
+ *E-mail: abdelrahmanbasil@yahoo.com & abdelrahmanbasil@uomosul.edu.iq*
1021-9986/2023/1/139-154 16/$/6.06

INTRODUCTION

Pharmaceutical Drugs (PDs) have been widely exhausted to guarantee a healthy state for individuals and vetenery[1]. Recently, discharging PDs into the environment, particularly into the aqua-resources, has increased. The entry of these organo-compounds into the aqua system, namely freshwater bodies, is associated with a series of environmental concerns due to their long-term influences on the aquatic environment[2]. Antibiotics, painkillers, analgesics, and hormonal drugs, are the most PDs that might be occurred in water. The sewage systems of hospitals, drug manufacturing units, and private households, are the primary sources for the PDs in water [3-5]. The presence of these chemicals in the aquatic environment, even though in low concentrations, causes a real probable long-term danger for marine and global creatures, because they aren't implemented in the metabolism, and thus, excreted to the eco-system, leading to the contamination of both ground and surface water resources[6].

Antibiotics (ABs) are among the most effective PDs employed as a medicine for humans and veterinary, to inhibit and treat infections, are antibiotics (ABs). The production of ABs worldwide increased and reached up to 11100 per year in 20 countries[2]. ABs are employed as a growing aspect of fish farms and livestock. They are also utilized for killing target microorganisms, even when utilized in low doses. It was reported that the number of ABs kinds used in human and veterinary medicine had exceeded 250[7]. Due to their weakly absorption by the human body, ABs are either converted or unaffected and finally excreted in faeces and urine[8]. Classification of ABs was performed based on their mechanism of action or chemical composition[9]. The concentration of ABs in wastewaters reached up to 400 mg/L[2].

Their high resistance to biodegradation encouraged the application of varied techniques to remove ABs from wastewaters, including photo-degradation, photophenton, electrocoagulation, ozonation/H_2O_2, membrane technologies, and adsorption [4,10-14]. Nevertheless, adsorption is the most widespread technique employed to eliminate ABs from wastewaters due to its efficiency and simplicity. Furthermore, it is easy to work and measure, eco-friendly, does not cause secondary contamination, and also cheap[15-17]. Multiple adsorbents, such as carbon-based adsorbents [18-22], molecular imprinted polymers[23], metal oxide [24], minerals and clay[25], chitosan and gels[26], and synthetic resins[27,28] have been utilized in eliminating various ABs and other pollutants from wastewaters.

The utilization of natural clays (NCs), such as bentonite, kaolinite, illite, and montmorillonite as adsorbents in eliminating the organic contaminants from wastewaters was achieved due to they owned many merits over other adsorbents, including availability, non-toxicity, porosity, high prospective for ion exchange, significant adsorption feature, pH, the possibility of surface modification, besides their low price[29,30]. Also, these NCs can eliminate numerous impurities from wastewater either through adsorption or by ion-exchange or both[31].

Numerous natural clays (NCs) and modified clays have been employed as adsorbents for ABs elimination from wastewater. *Farajfaed et al.* [32] investigated the elimination of levofloxacin and gemifloxacin from their aqueous solutions using the granular silica pillared clay. The adsorptive removal of metronidazole overlay aggregate covered by MgO nanoparticles was established in the literature [33]. Verde-lodo bentonite clay was implemented as an adsorbent to eliminate Ofloxacin from its aqueous solution in the batch and fixed-bed systems [34]. Finally, thermally modified bentonite clay was utilized as a priceless adsorbent for ciprofloxacin removal from the aqueous solution[35].

Among the semi-synthetic ABs is Rifampicin (RIFA). This antibiotic possesses a complicated structure, and it composes of an aliphatic bridge linking two non-adjacent locations of an aromatic nucleus. RIFA is the chief medicine for curing tuberculosis, necessitating a long-term cure (6–9 months) with high dosages. It was also employed for curing immunosuppressed patients, and therefore, it is a potential drug for essential health care. When RIFA is utilized as a drug, its remaining is discarded by humans through urine, which is, in turn, ejects into the wastewater [36-38].

Among the NCs that were widely employed for the adsorption of various pollutants from wastewater is, red mud (RM). It is one of the most famous available and priceless NCs. It can occur in rocks as crystalline structures worldwide. The kaoline RM essentially composes of kaolinite, besides some other minerals, including mica and quartz. The kaolinite surface is characterized by bearing a fixed structural negative charge originates from the

isomorphous replacement of Si^{+4} by Al^{+3} in the silica layer, which acts as the energetic site to adsorb the organic and inorganic pollutants [39,40]. It was widely implemented as a priceless adsorbent for removing various contaminants from contaminated waters. The Iraqi RM kaolinite was implemented as a cheap adsorbent in methyl blue elimination from its aqueous solution [39]. The Algerian kaolinite was tried as a priceless adsorbent to remove methylene blue from wastewater [41]. *Xing et al.* [42] inspected the red loess to eliminate heavy metals from the polluted waters. The natural and activated forms of the RM were implemented as a low-cost adsorbent for eliminating heavy metals, including Pb, Cd, and Zn, from their aqueous solution [43].

Investigations related to the adsorptive removal of RIFA using different adsorbents are limited. *Henrique et al.* [44] used calcined *Mytella falcata* shells as a priceless sorbent for excluding RIFA from its aqueous solution. The adsorptive elimination of RIFA by iron nanoparticles synthesized by a tea extract was also established in the literature [38]. Recyclable nano-Fe_3O_4 was inspected as a sorbent to adsorb RIFA from its aqueous medis [44]. However, implementing the RM or the activated RM in ABs elimination or RIFA from the contaminated waters are infrequent. Therefore, this paper explores the possibility of examining the Acid-Activated Iraqi Red Mud (AIRM) as a possible adsorbent in removing RIFA from synthetic wastewater. After the acid activation of the IRM, it was identified by several techniques, and then employed in RIFA elimination from its aqueous solution. The influence of adsorption operative factors, like solution's pH, initial concentration of RIFA, sorbent dosage, temperature, and the adsorption duration on RIFA adsorption by the AIRM, was investigated. Diverse kinetic and isotherm models for RIFA adsorption onto the sorbent were examined and discussed.

EXPERIMENTAL SECTION

Chemicals and materials

Analytical grade hydrochloric acid (HCl, 37.0%) and sodium hydroxide (NaOH, pellets, 99.9%) were purchased from Scharlau chemicals, Spain. Rifampicin (RIFA, $C_{43}H_{58}N_4O_{12}$) with a purity of 97% was acquired from MEDOCHEMEI, LIMASSOL, CYPRUS. The Iraqi Red Mud (IRM) samples were brought from the Al-Abassiyah region, northwest Mosul city, Nineveh Government, Iraq. All experiments were accomplished utilizing De-ionized Water (DW).

Preparation of adsorbent

The IRM samples were mixed, pulverized, and then sieved by a 0.074 mm sieve. The clay particles were then mixed with a solution of 10% HCl. The mixture was refluxed with stirring for 5h at 600 rpm stirring rate. By the end of the reflux, the mixture was left to cool, filtered, and washed with boiled DW until neutral water was attained. Next, it was dried at 110 °C until reaching a fixed weight. Finally, the Activated Iraqi Red Mud (AIRM) was sieved to obtain a uniform particle size and kept in a tight container for further identification and use.

Characterization of the AIRM

Divers techniques were employed to diagnose the parent IRM and the AIRM. The samples' morphological characteristics, along with their elemental analysis, were achieved by Field-Emission Scanning Electron Microscope-Energy Dispersive X-ray analyzer (Tescan Mira 3 LMU FESEM-EDX, France, 2018). The BET surface area (SA_{BET}), N_2 adsorption/desorption isotherms at 77 K, and the pore volume of the IRM and AIRM were determined on a BELSORP MINI II, Japan, surface area and porosimetry analyzer. The crystallinity of the samples was inspected by a high-resolution X-ray diffractometer system (Malvern Panalytical X-ray diffraction, UK) with Cu kα radiation (λ) of 0.154 nm at 40 kV and 20 mA in the 2θ range of 10 ° to 90 °. The characteristic functional groups on the IRM and AIRM surfaces were determined on a Fourier Transform Infra-Red spectrophotometer (FTIR JASCO V-630, USA) at a wavelength of 4000 – 400 cm^{-1} employing KBr pellets at a resolution of 4 cm^{-1} and 32 cm^{-1} scans. The point of zero charges (pHpzc) for the AIRM adsorbent was determined following the procedure given elsewhere [45].

Adsorption studies

Batch experiments were accomplished to analyze the influence of diverse experimental conditions on the amount of RIFA adsorbed by the AIRM. A pre-determined amount of the adsorbent was added into a 250 mL- glass bottle containing a100 mL of the effluent solution. The mixture was then agitated until attaining equilibrium. The effect of the effluent pH was inspected by changing

the pH from 2.0 to 10.0 by the drop-wise addition of 0.10 M HCl or 0.10 M NaOH, using a stock solution of 300 mg/L, 0.15 g of the adsorbent at 35 °C for 180 min. The influence of RIFA initial concentration (50-300) mg/L), AIRM dosage (0.1 – 0.30 g), contact time (30-210 min.), and temperature (35 °C, 45 °C, and 55 °C) on the amount of RIFA adsorbed were investigated. The sorbent particles were separated from the solution by centrifugation, and the residual RIFA concentration in the supernatant was sepcifed by UV–vis spectrophotometer at 475 nm. Each experiment was repeated at least twice, and the value was presented as the mean± SD. The initial and final concentrations of RIFA were measured. The amount of adsorption at equilibrium, qe (mg/g), was calculated utilizing the following formula:

$$q_e = \frac{(C_o - C_e)\,V}{W} \quad (1)$$

where, C_o and C_e are the initial and equilibrium concentration of RIFA (mg/L), V represents the volume of the solution, and W refers to the mass of the AIRM utilized (g). The removal percentage of RIFA (RIFA %) was determined as follows:

$$\text{RIFA}(\%) = \frac{(C_o - C_e)}{C_o} X\ 100 \quad (2)$$

Adsorption isotherms

The adsorption data of RIFA by the AIRM were fitted to the Langmuir formula, which suggests monolayer adsorption and also to Freundlich model, which refers to multilayer-adsorption. The Langmuir linearized forms of the adsorption formulas were applied to express the monolayer adsorption, which demonstrates the existing steps about randomly adsorbing RIFA molecules onto the AIRM surface[46]. The following formula expresses the linear form of the Langmuir model:

$$\frac{C_e}{q_e} = \frac{1}{q_m K_L} + \frac{C_e}{q_m} \quad (3)$$

Where, C_e (mg/L), q_e (mg/g), q_m (mg/g), and K_L are the RIFA equilibrium concentration (mg/L), amount of RIFA adsorbed per gram of the AIRM (mg/g), amount of RIFA needed to form a mono layer on the AIRM surface (mg/g), and the Langmuir constant (L/mg), respectively. Plotting C_e (mg/L) versus C_e/q_e (L/g) will give q_m and K_L. The separation factor (R_L), which offers the Langmuir isotherm characteristic, can be determined utilizing the following expression:

$$R_L = \frac{1}{1 + C_0 K_L} \quad (4)$$

The Freundlich experimental equation refers to multi-layer adsorption, suggesting that the adsorption positions' heterogeneity is located on the adsorbent surface[46]. The basis of the linear form of the Freundlich model of adsorption is given in the following equation:

$$\ln q_e = \ln K_F + \frac{1}{n} \ln C_e \quad (5)$$

Where, K_F represents the adsorption capacity (mg/g), while 1/n relaates to the adsorption intensity (g/L). The constants n, and K_F could be deduced from the slope and intercept of the Freundlich isotherm's liner plot.

Adsorption kinetics

The adsorption kinetic mechanisms, namely the pseudo-first-order and pseudo-second-order models of RIFA adsorption by the AIRM have also investigated. The pseudo-first-order kinetic equation is given in Eq. (6):

$$\ln(q_e - q_t) = \ln(q_e) - k.t \quad (6)$$

Where, *qt* (mg/g) and *qe* (mg/g) are the adsorbed amount of RIFA at the equilibrium time (t_e), respectively, while *k* (min^{-1}) is the pseudo-first-order rate constant, respectively. The linear expression of the pseudo-second-order kinetic model is illustrated in Eq. (7):

$$\frac{t}{q_t} = \frac{1}{k_2 {q_e}^2} + \frac{t}{q_e} \quad (7)$$

Where, k_2 (g/mg.min) is the pseudo-second-order rate constant.

RESULT AND DISCUSSION

Characterization of IRM and AIRM

The IRM before and after the acid treatment was identified by several techniques to detect the alteration occurred in its chemical and textural features as a result of the acid treatment.

The elemental analysis determined by the EDX technique of the authentic IRM before and after the acid treatment are given in Fig.1. The results exhibited that Mg, Al, Si, Ca, Fe, and K were the main elements forming the IRM. After the acid treatment, the concentration of Mg,

Table 1: BET surface area and pore volume of the RM and AIRM.

Property	IRM	AIRM
BET surface area (m^2/g)	30.99 ± 1.50	60.96 ± 1.50
Langmuir surface area (m^2/g)	31.89 ± 1.00	63.45 ± 1.50
t-Plot micropore area (m^2/g)	27.36 ± 1.50	55.14 ± 1.50
V_{total} ($cm^3\ g^{-1}$)	0.0949 ± 0.0004	0.1621 ± 0.0011
Mean pore diameter (nm)	12.26 ± 0.25	10.63 ± 0.27

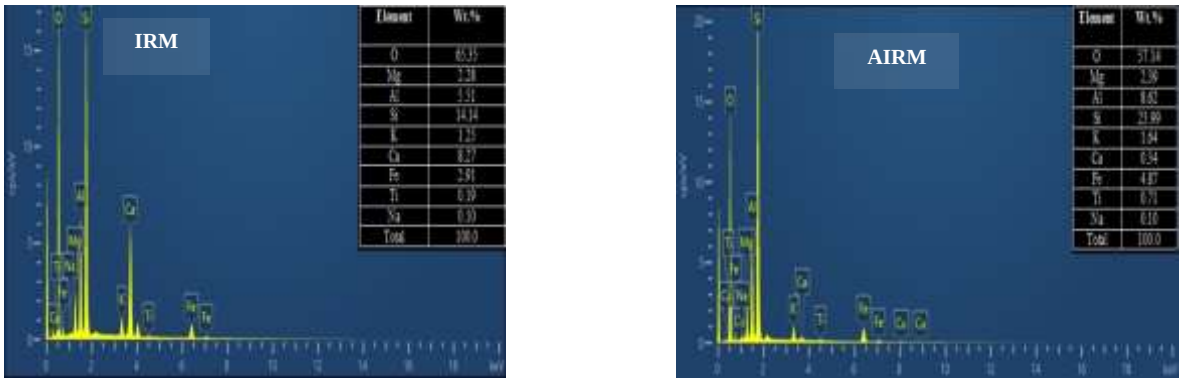

Fig. 1: EXD analysis of the IRM and AIRM.

Al, Si, K, and Fe increased, while the Ca concentration diminished from 8.27% to 0.32% as a consequence of the amorphization of the clay mineral because of pre-tretment with acid resulting in the formation of more amorphous silica[47].

Table 1 offers the SA_{BET} and pore volume of the IRM and its activated sample. The SA_{BET} of the pristine IRM was 30.99 m^2/g. This value is higher than that reported for the Algerian kaolin clay 21.27 m^2/g[41] and the Indian kaolin clay 13.69 m^2/g [48]. After the acid activation, the SA_{BET} raised to 60.96 m^2/g. This finding may ascribe to the elimination of some metal oxides during the acid treatment, such as the CaO, which its concentration declined from 8.27% to 0.34%[47].

The pore volume reduced from 12.26 nm for the IRM to 10.63 nm for its activated sample. Furthermore, the IRM has a mesoporous structure according to IUPAC classification [49]. The N_2 adsorption/desorption isotherm of the samples are illustrated in Fig. 2. Following the IUPAC classification, the N_2 adsoprtion-desoption isotherms are related to the typical type IV with a type H1 hysteresis loop as a result of the mesoporous structures of both samples[39].

The crystal phase patterns of the IRM before and after modification, have been determined by the XRD, and the results are displayed in Fig.3**.** It was found that hematite (α-Fe_2O_3), goethite (α -FeO(OH)), gibbsite (γ-$Al(OH)_3$), calcite ($CaCO_3$), rutile/anatase (TiO_2), and quartz (SiO_2), are the main mineral phases that forming the IRM and its modified sample. Nonetheless, after treating the IRM with acid, Calcite was nearly removed along with other components, which in turn raised the SA_{BET} of the attained acid modified sample.

Fig.4 illustrates the FT-IR spectrum of IRM and the AIRM. The spectrum shows that the sharp absorption bands at 3700-3600 cm^{-1} in pre and post adsorption indicate the stretching vibrations of water hydroxyl (O–H) groups in magnesium, iron, aluminum, and silica oxide/hydroxide besides the molecular water adsorbed on their surface. The bands at 1641 cm^{-1} attribute to the hydroxyl group bending modes of the inter-layer adsorbed molecules of H_2O. The bands observed in the range of 1006–873 cm^{-1} are connected to the Si–O–Si bond stretching vibrations[50-52]. Similarly, the bands observed in the range of 801and 873 cm^{-1} relate to the stretching vibrations in Fe–OH and CaO, respectively[50-52].

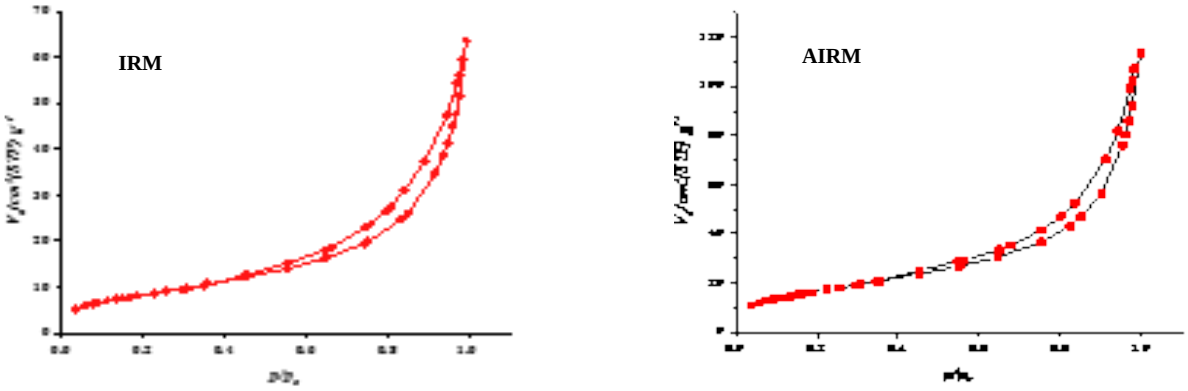

Fig. 2: N_2 adsorption/desorption isotherms of N_2 gas over the IRM and AIRM.

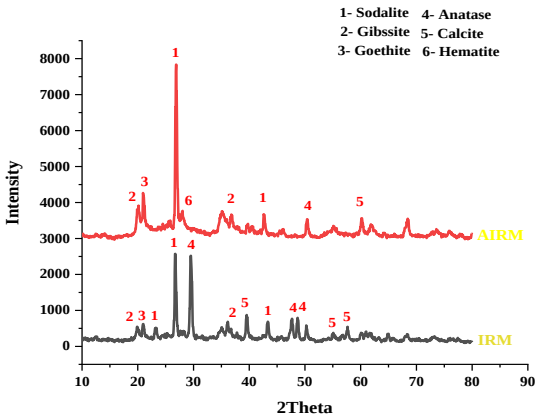

Fig. 3: The XRD patterns of the IRM and AIRM.

The absorption peaks at 1423-1458 cm^{-1} ascribe to (O–C–O) asymmetric stretching vibrations[48]. The broad peak fixed at 997 cm^{-1} was assigned to the asymmetric stretching vibration of Si–O[53]. The bands at 875 cm^{-1} and 779 cm^{-1} are attributed to the presence of calcite[43]. Two bands in the regions of 685 cm^{-1} and 557 cm^{-1} were due to the symmetric and bending vibration of Si–O–Al framework, respectively[50], which confirmed the presence of Na–zeolite in IRM. Moreover, the appearance of a peak at 460 cm^{-1} was ascribed to stretching vibrations of the Fe–O bond in hematite[48].

The FESEM technique was implemented to examine the surface morphology and microstructure of the raw IRM and its modified adsorbent.

It is notable from Fig.5, which illustrates the FESEM image of the IRM surface that its surface composes of multiple-size hexagonal flakes besides fragmented edges. After the acid treatment, pores with various sizes and shapes were formed. Also, some flakes were also seen on the acid-treated IRM surface. In addition, there were some whilst deposited on those flakes, which may belong to the oxides of magnesium, sodium, calcium, potassium, iron, etc[47].

Adsorptive removal of removal of RIFA by the AIRM

The adsrorptive elimiantion of RIFA by the AIRM was investigated through inspecting varibels affecting its removal effecncy, like the solution initial pH, RIFA initial concentration, AIRM amount, tmperautre, and contact time.

The adsorption of RIFA by the AIRM was investigated at various pH in the range of 2.0 to 9.0 using 100 mL of (300 mg/L) RIFA concentration at 308 K and an adsorbent dosw of 0.25 g. Fig.7 illustrates that lessening the solution pH caused an enhancement in the amount of RIFA adsorbed. The highest adsorption capacity of RIFA achieved at a pH of 4.0. The higher values of pH lessened the RIFA adsorption capacity. This result may ascribe to the fact that increasing the solution pH results in a reduction in the positive charges on the RIFA molecules, leading to a decline in the electrostatic attraction between the RIFA molecules and the adsorbent surface. So, the RIFA adsorption deminished[53]. The RIFA adsortion capaity declined as the pH exceeded 4.0, because of the increment of the OH^- ions concnetration in the solution as well as the nageagive charge raising on the AIRM surface. This will lead to a a negative interaction betwenn the RIFA ions and the AIRM surface, resulting in a prohibition of RIFA adsorption[44].

The AIRM possessed a pHpzc value of 7.60 as depicted in Fig.7. Overall, when the pH value exceeds the pHpzc, the AIRM surface will cary negative charges, and thus causing a strong electrostatic attraction between negative surface charge of sorbent and the RIFA cations.

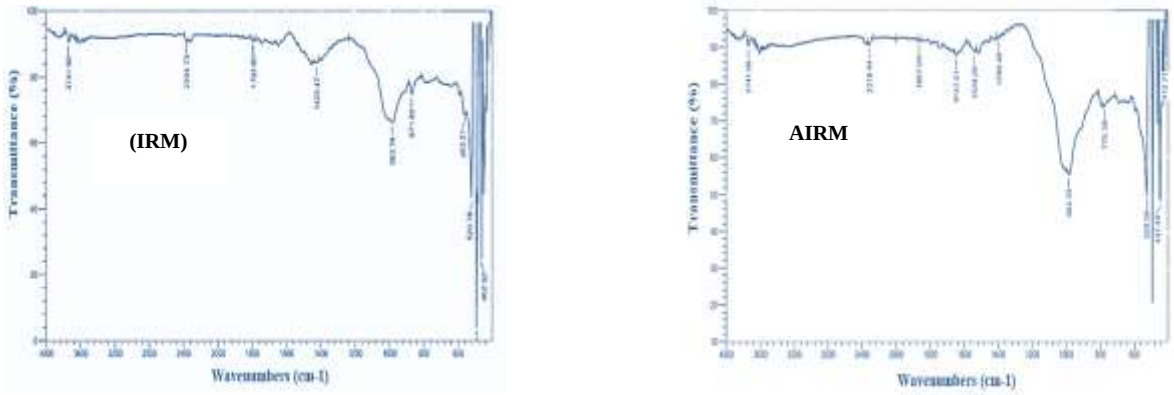

Fig. 4: The FT-IR spectra of the IRM and AIRM.

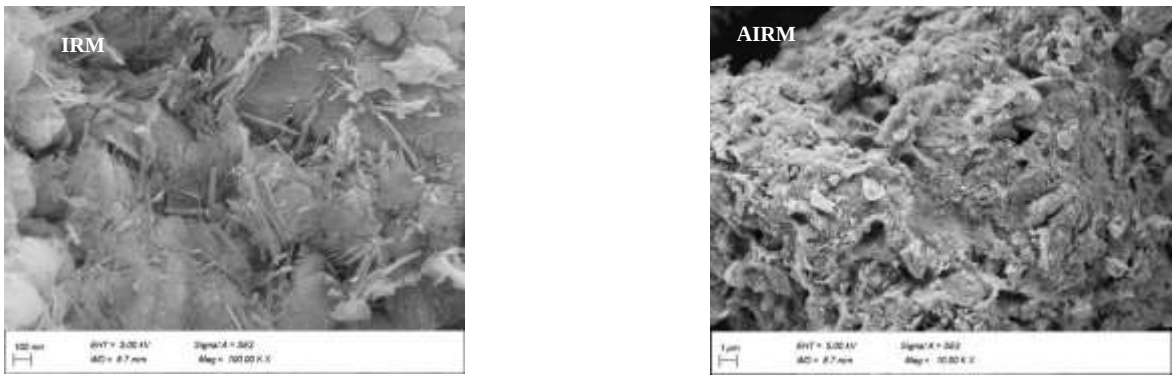

Fig. 5: FESEM images of the IRM and AIRM.

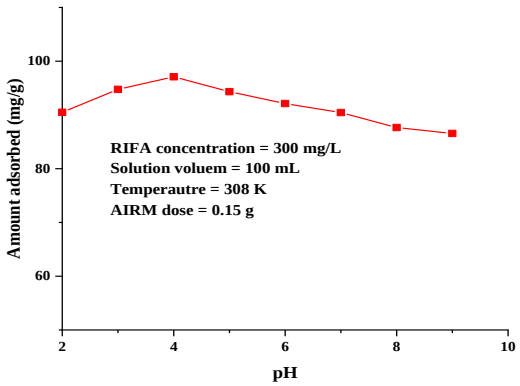

Fig. 6: Effect of pH on the adsorptive elimination of RIFA by the AIRM.

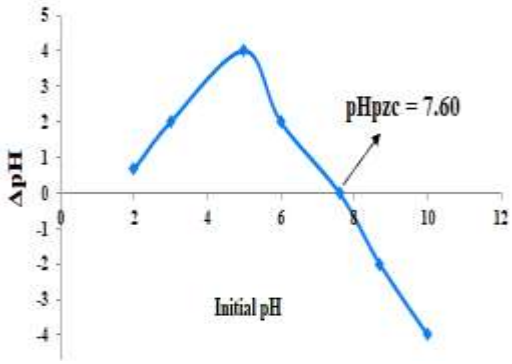

Fig. 7: The pHpzc of of the AIRM.

On the contrary, if the pH value is below the pHpzc, the AIRM surface will carry a portive charges, which results in a repusion among the RIFA cations and the positive charge of the sorbent surface, causiing a deminish in the RIFa removal %[54].

The initial concentration of the adsorbate offers a significant motivating force to bypass the mass transfer oppositions of the adsorbate molecules between the aqueous and solid phases. Thus, the adsorption enhances with the increment of the initial concentration of the adsorbate[54]. The influence of the RIFA initial concentration (50–300 mg/L) on its adsorbed amount

using 100 mL of RIFA solution, 0.10 g of the AIRM at 308 K and a pH of 4.0 was examined. Fig. 8 revealed that the amount of RIFA adsorbed (q_e) increased from 25.0 mg/g to 150.0 mg/g as the RIFA initial concentration raised from 50 mg/L to 300 mg/L. This outcome ascribes to the fact that increasing the RIFA initial concentration will increase the concentration difference between the solution and the absorbent surface. It also raises the driving forces responsible for the mass transfer, causing the adsotion of more RIFA molecules[55].

Investigating the impact of the amount of the AIRM utilized on the adsorption capacity of RIFA was inspected by testing various doses of the AIRM in the range of 0.10 g to 0.30 g. These experiments were accomplished using 100 mL of 300 mg/L RIFA initial concentration at 308 K and a pH of 4.0. The consequences offered in Fig.9 illustrates that the adsorbed amount of RIFA increased with increasing the AIRM dose. This outcome suggests that the higher doses of the AIRM provide much greater total surface area as well as more active sites for attracting RIFA molecules[44,54]. Nonetheless, amounts over 0.20 g had an insignificant impact on the adsorptive capacity of RIFA due to the removal of most of RIFA molecules by the typial amount of the AIRM. Thus, an amount of 0.20 g was chosen for subsequent experiments.

The impact of temperature on adsorption uptake of RIFA using the AIRM was inspected in the temperature range of 308 K – 328 K. The experiments were completed using 100 mL of 300 mg/L RIFA initial concentration at a pH of 4.0 and 0.20 g of the AIRM. Fig.10 implies that RIFA adsorption has increased with rising temperature. This is mainly because increasing temperature increases the system entropy, causing more collisions among the RIFA molecules and the adsorbent particles, resulting in an enhancement in activities at the interface between the adsorbent and adsorbate[56]. Moreover, increasing the process temperature decreases the solution's viscosity, making the collisions among the adsorbate molecules and the adsorbent particles easier, leading to better removal of the pollutant[56]. The increment of RIFA adsorption by the AIRM assures the endothermic nature of the adsorption process.

The contact period effect on the adsorptive capacity of RIFA by the AIRM was studied at various time intervals in the range of 30 –180 minutes, as also illustrated in Fig.10. The adsorption experiments have been performed

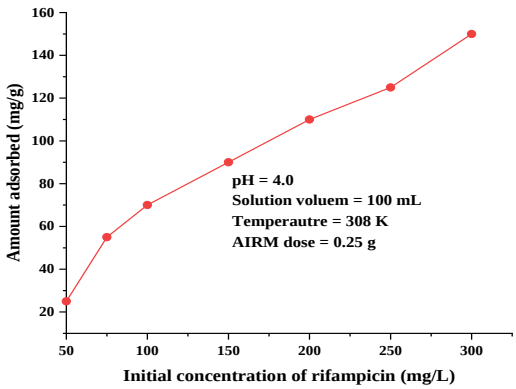

Fig. 8: Effect of RIFA initial conncetration on its amount adsorbed by the AIRM.

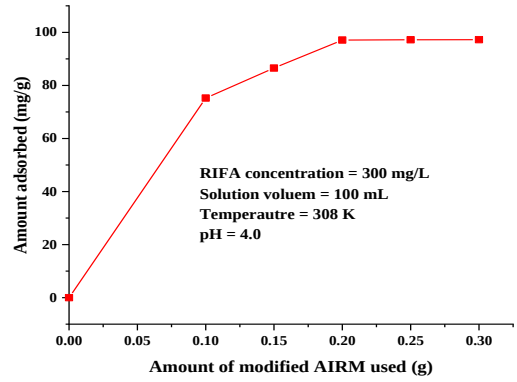

Fig. 9: Effect of the AIRM dose on the amount of RIFA adsorbed by the AIRM.

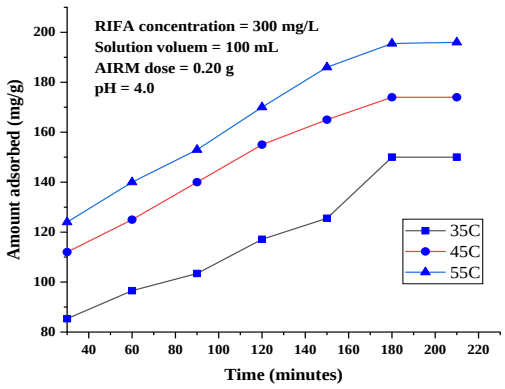

Fig. 10: Effect of temperatureon and contact time on the amount of RIFA adsorbed by the AIRM.

Table 2. Langmuir and Freundlich constants of RIFA adsorption by the AIRM at various temperatures.

Temperature (K)	Langmuir				Freundlich		
	q_m (mg/g)	K_L (L/mg)	R_L	R^2	n	K_F (mg/g)	R^2
308	160.97	0.0531	0.0590	0.9844	2.43	1.11	0.8712
318	195.69	0.0411	0.0411	0.9921	2.18	1.08	0.9619
328	217.93	0.0451	0.0451	0.9931	2.28	1.16	0.9117

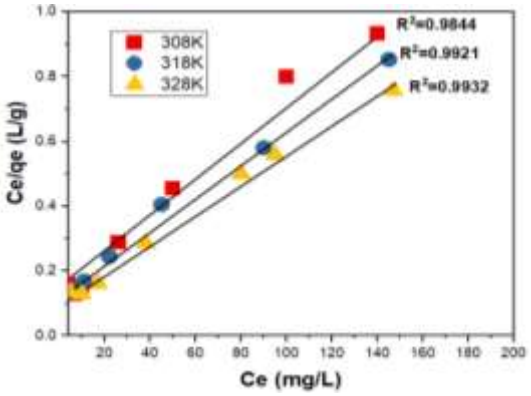

Fig. 11: Langmuir adsorption isotherm of RIFA adsorption by the AIRM.

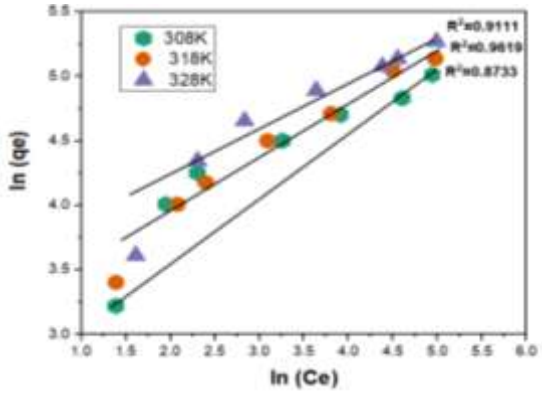

Fig. 12: Frendlich adsorption another of RIFA adsorption by the AIRM.

at the optimal conditions obtained previously. The results exhibited that the adsorptive capacity of the RIFA increased with increasing the contact period so that the RIFA adsorption by the AIRM was good at the first 30 min., suggesting that it is spontaneous. This outcome ascribes that the adsorption is very fast in the early stages because of the larger surface area of the adsorbent accessible to adsorb the RIFA molecules. The equilibrium was attained after 180 minutes. When the balance is attained, the active sites will be occupied by RIFA molecules, and the active positions will be entirely unavailable. They may create a repulsive force between the adsorbate on the adsorbent surface and in the bulk phase[46].

Adsorption equilibrium

Adsorption isotherms are commonly utilized to inspect the equilibrium parameters and the adsorption features besides providing an insight into the nature of interactions between the adsorbent and the adsorbate[37]. The Langmuir and Freundlich isotherms, which are respectively illustrated in Fig.11 and Fig.12), were applied to explain the adsorption data of RIFA by the AIRM.

The slope and intercept of plotting C_e/q_e vs. Ce gives the Langmuir constants q_m and K_L, respectively, while the slope and intercept of plotting ln (C_e) vs. ln (q_e) yields the Freundlich constants, n and K_F, respectively.

Analyzing those models' correlation coefficient (R^2) suggested that the adsorption is monolayer as it obeyed the Langmuir model rather than the Freundlich model. This conclusion was drawn following the R^2 values, which was higher for the Langmuir model than that of the Freundlich model [38]. The constants relating to the Langmuir and Freundlich isotherms, which are offered in Table 2 exhibited that the R_L value of the Langmuir model of adsorption suggests that RIFA adsorption onto the AIRM is favorable due to its value, which was $0 < R_L < 1.0$. The value of n in the Freundlich isotherm was above 1.0, suggesting that the adsorption of RIFA over the AIRM is beneficial.

Kinetic studies of RIFA adsorption over AIRM

The adsorption kinetics of RIFA antibiotic by the AIRM was examined by analyzing the adsorption data following the pseudo-first-order and pseudo-second-order models of kinetics, as shown in Fig.13 and Fig.14, respectively.

Table 3: Pseudo-first-order and pseudo-second-order kinetic models constants of RIFA adsorption by the modified AIRM at various temperatures.

Temperature (K)	Pseudo-first-order model			Pseudo-second-order model		
	k_1	q_{e1} (mg/g)	R^2	k_2	q_{e2} (mg/g)	R^2
308	0.0115	1.59	0.8728	0.00010	181.18	0.9523
318	0.0083	1.42	0.9779	0.00013	200.23	0.9935
328	0.0090	6.53	0.9730	0.00015	227.79	0.9902

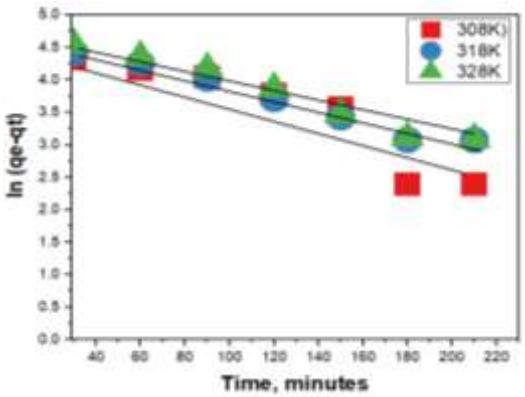

Fig. 13: The pseudo-1st-order kinetic model of RIFA adsorption by the AIRM.

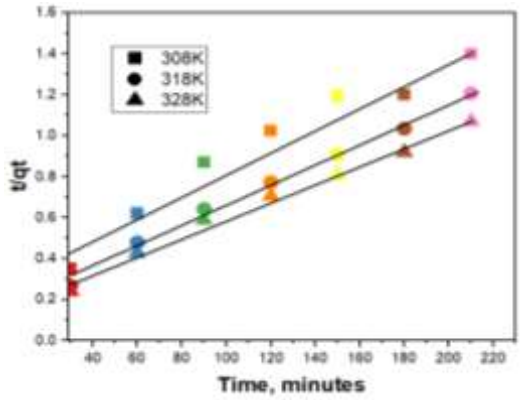

Fig. 14: The pseudo-2nd -order kinetic model of RIFA adsorption by the AIRM.

The kinetic studies were investigated at a temperature range of 308 -328 K. The kinetic model outcomes disclosed that the pseudo-second-order model could better explain the RIFA adsorption onto the AIRM due to its R^2 value (0.9902), which was above that obtained for the pseudo-first-order (0.9730). The consequences are in line with those announced for RIFA adsorption by the iron nanoparticles synthesized by a tea extract [38] and recyclable nano-Fe_3O_4[44]. As the pseudo-second-order model postulates that chemisorption is the rate-limiting step, it could be said that the interaction between the antibiotic molecules and the modified AIRM are either by charge neutralization or electrostatic attraction[38,44]. Table 3 offers the constants related to the pseudo-first-order model and pseudo-second-order model.

Adsorption thermodynamics

Thermodynamics functions (ΔH, ΔS, and ΔG) of RIFA adsorption by the AIRM at 300 mg/L initial concentration of RIFA were determined by batch studies at diverse temperatures (308 K,318 V, and 328 K). Calculating thermodynamic functions was accomplished using the following equations [57-60]:

$$\ln(K_c) = \frac{\Delta S_o}{R} - \frac{\Delta H_o}{RT} \quad (8)$$

$$\left(\frac{q_e}{C_e}\right) = K_c \quad (9)$$

$$\Delta G_o = -RT \ln K \quad (10)$$

Where, ΔS_o (kJ/mole K), ΔH_o (kJ/mole), ΔG_o (kJ/mole), *K*, and *R* are the standard change in entropy, change in enthalpy, and Gibbs free energy, equilibrium coefficient, and the universal gas constant (8.314 J/mol), respectively. The liner plot of 1/T vs. ln q_e/C_e gives ΔH_o and ΔS_o, which could be calculated from the slope and intercept of the plot. The thermodynamic functions values presented in Table 4 specified that the adsorption of RIFA by the AIRM was endothermic (ΔH_o =7.57 kJ/mole), suggesting that the RIFA adsorption by the AIRM is temperature-dependent, and also spontaneous due to the negative value of ΔG_o.

Comparison of RIFA adsorption with other adsrobents

Table 5 lists a comparison of RIFA adsorption outcomes by the AIRM with those established for its adsorption by other adsorbents in the literature as well

Table 4: Thermodynamic parameters for RIFA adsorption on AIRM.

ΔH_o (kJ/mole)	ΔS_o (kJ/mole K)	ΔG_o (kJ/mole)		
		308 K	318 K	328 K
7.57	8.16	−0.1732	−0.4150	−0.6940

Table 5: Comparison of RIFA adsorption capacity by different adsorbents.

Adsorbent	Amount of RIFA adsorbed (mg/g)	Reference
Hybrid rGO@Fe/Pd nanoparticles	90.09	[61]
Cocoa shells	26.66	[49]
Nano-Fe	107.70	[38]
Calcined Mytella Falcata Shells	10.00	[37]
AIRM	227.79	This work
Raw IRM	87.22	This work

as the authentic IRM. It can be seen from Table 5 that the AIRM had the highest adsorptive capacity for RIFA in comparison with different adsorbents. This variation in the adsorbed amount of the antibiotic could ascribe to various factors, such as the surface area and pore volume of the adsorbent, types of functional groups that occurred onto its surface, the initial concentration of the antibiotic, amount of the adsorbent used, as well as the type of the adsorption mechanism.

For comparison, the authentic IRM was tried as an adsorbent for the elimination of RIFA from its aqueous media by applying the optimal conditions obtained using the AIRM (100 mL of 300 mg/L RIFA, 0.20 g of the adsorbent, pH of 4.0 at 328 K for 180 minutes contact time). The outcomes exhibited that RIFA elimination by the AIRM was better than the pristine IRM. This variation in the adsorptive capacities between the two sorbents is expected because the higher SABET of the AIRM than the prestine IRM.

Adsorption mechanism

Varied influential adsorption positions like the aluminol (–Al–O–H), as well as the silanol (– Si–OH) and the hydroxyl (–O–H) groups on the mineral edges, could be occurred on the AIRM surface [38]. The presence of theoe effective groups have bee confirmed by the FT-IR spectra,as illustrated in Fig.4. Additionally, these groups play a vital role in the adsorptiv eliination of RIFA by the AIRM. Many mechanisms could participate in the interactions between the RIFA molecules and the AIRM surface. Following the adsorption kinetics and isotherms results, the adsorption of RIFA occurs predominantly through the chemical interaction because of the attachment of the RIFA active groups with the AIRM surface groups. As the RIFA adsorption is pH-dependent (maximum adsorption was at pH= 4.0), the RIFA is found in a zwitterionic form. The electrostatic interaction is another probable mechanism between the RIFA cations and the negative charges over the AIRM surface. The H-bonding interactions could be another possible mechanism that could be happened between the H atom existing on the AIRM surface (Al–O–H, – Si–O–H, and (–O–H) and the N atom in the RIFA molecules. The last probable mechanism is the n-τ interaction, which arises from the delocalization of the oxygen atoms pair electrons into the τ orbital of the RIFA aromatic rings[45]. Therefore,

it can be said that the RIFA adsorption by the AIRM was influential in the presence of the above interaction mechanisms. Fig.15 illustrates the proposed mechanism for RIFA adsorption by the AIRM.

Reusability study

One of the essential criteria that encourages the practical exploitation of an adsorbent is its recyclability. Here, the spent AIRM was treated with ethanol in a Soxhlet extractor, washed with deionized water, and then activated at 110 °C for 5h. The regenerated samples were implemented in removing RIFA under the optimal conditions obtained previously (100 mL of 300 mg/L, 0.20 g of the AIRM at 328 K for 180 minutes and a pH of 4.0).

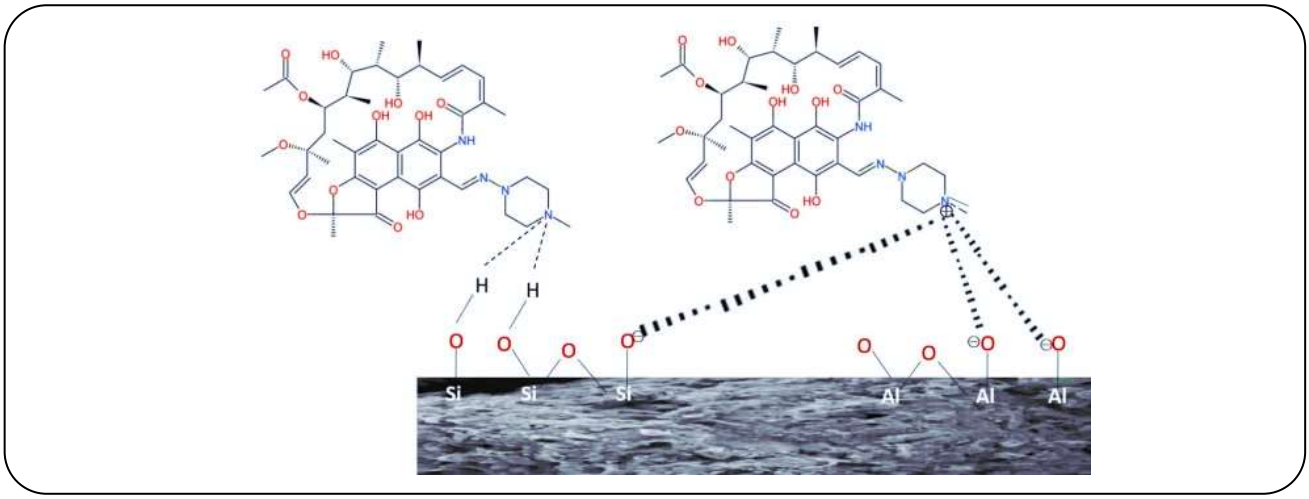

Fig. 15: The proposed mechanism for RIFA adsorption by the AIRM.

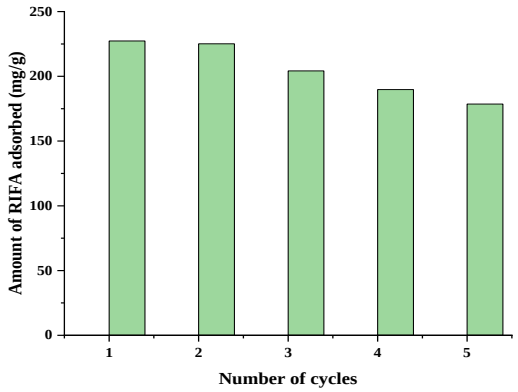

Fig. 16: Effect of reusability of ARM on RIFA adsorption.

The consequences showed that the regenerated sample effectively eliminated the antibiotic with a good adsorption capacity even after 5 cycles, suggesting that it is highly reusable. Fig.16 demonstrates the impact of the reusability of the AIRM on RIFA adsorption.

CONCLUSIONS

The current investigation indicated that the acid treatment of the raw IRM increased its surface area from 30.99 m^2/g to 60.96 m^2/g. Besides, the utilization of the AIRM has proven its ability on removing RIFA antibiotics from its aqueous solution with a maximum removal capacityof (217.93 mg/g) at an initial pH of 4.0 using 0.20 g of the AIRM at 328 K for 180 minutes contact time. The Langmuir adsorption isotherm was best fitted to the sorption data of RIFA by the AIRM than the Freundlich model due to the higher R^2 value of the former (R^2 =0.9902) than that of the latter (R^2 = 0.9730). In addition, the adsorptive elimination data of RIFA by the AIRM were best described by the pseudo-second-order kinetic model than the pseudo-first-order kinetic model because of the higher *R2* value of the former (R^2 = 0.9902) than that of the latter (R^2 = 0.9730). The adsorption of RIFA by the AIRM was spontaneous due to the negative value of ΔG, which its values were between − 0.1732 and − 0.6940 kJ/mol at various temperatures. Besides, chemisorption was the dominant adsorption mechanism. Finally, the reusability examination of the regenerated AIRM showed that the sorbent effectively adsorbs RIFA for 5 cycles with a good capacity.

Aknlowdgmnets

The authors would like to express their sincre thank to Chemistry Department, Mosul University, Iraq for presenting research facilities to achieve this investigation. We declare no conflicts of interest.

Received : Oct. 29, 2021 ; Accepted : Jan. 31, 2022

REFERENCES

[1] Grenni P., Ancona V., Barra A., Ecological Effects of Antibiotics on Natural Ecosystems: A Review, *J. of Microchem*, **136**:25–39(2018).

[2] Masoudi F.S., Kamranifar M., Naghizadeh A.., Efficiency of Chitosan Extracted from Persian Gulf Shrimp Shell in Removal of Penicillin G Antibiotic from Aqueous Environment, *Iran. J. Chem. Chem. Eng. (IJCCE)*, **39(4)**: 235-244(2020).

[3] Mackulaka T., Nagyová K., Faberová M., Grabic R., Koba O., Utilization of Fenton-like Reaction for Antibiotics and Resistant Bacteriaelimination in Different Parts of WWTP, *Environ. Toxicol. Pharmacol*,**40**:492–497(2015).

[4] Ahmed M.J, Adsorption of Quinolone, Tetracycline, and Penicillin Antibiotics from Aqueous Solution Using Activated Carbons: Review, *Environmental Toxicology and Pharmacology*, **50**:1–10 (2017).

[5] Oguz M., Mihciokur H., Environmental Risk Assessment of Selected Pharmaceuticals in Turkey, *Environ. Toxicol. Pharmacol*, **38**:79–83(2014).

[6] Bangari R.S., Sinha N., Adsorption of Tetracycline, Ofloxacin and Cephalexin Antibiotics on Boron Nitride Nanosheets from Aqueous Solution, *Journal of Molecular Liquids*, **293(111376)**:1-12 (2019).

[7] Trampe S.G., Ceapa C.D., Ruiz M.M., Sánchez S., Synthetic Biology Era: Improving Antibiotic's World, *Biochem., Pharmacol.*,**134**: 99–113(2017).

[8] Aydin S., Aydinb M.E., Beduk F., Ulvi A., Removal of Antibiotics from Aqueous Solution by Using Magnetic Fe_3O_4/red Mud-Nanoparticles, *Science of the Total Environment*, **670**: 539-546(2019).

[9] Ahmed M.B., Zhou J.L., Ngo H.H., Guo W., Adsorptive Removal of Antibiotics from Water and Waste Water: Progress and Challenges, *Science of the Total Environment*, **532**:112- 126(2015).

[10] Lu J., Sun J., Chen X., Tian S., Chen D., He C., Xiong Y., Efficient Mineralization of Aqueous Antibiotics by Simultaneous Catalytic Ozonation and Photocatalysis Using $MgMnO_3$ as a Bifunctional Catalyst, *Chem. Eng. J.*, **358**: 48-57(2018).

[11] Darweesh T.M., Ahmed M.J., Adsorption of Ciprofloxacin and Norfloxacin from Aqueous Solution onto Granular Activated Carbon in Fixed Bed Column. Ecotoxicology and Environmental, *Safety*,**138**:139–145(2017).

[12] Le T.H., Ng C., Tran N.H., Chen H., Gin K.Y.H., Removal of Antibiotic Residues, Antibiotic Resistant Bacteria and Antibiotic Resistance Genes in Municipal Wastewater by Membrane Bioreactor Systems,*WaterRes.*,**145**:498–508(2018).

[13] Zhu L., Santiago-Schübel B., Xiao H., Hollert H., Kueppers S., Electrochemical Oxidation of Fluoroquinolone Antibiotics: Mechanism, Residual Antibacterial Activity and Toxicity Change, *Water Res.*,**102**:52–62(2016).

[14] Sturini M., Speltini A., Maraschi F., Pretali L., Ferri E.N., Profumo A., Sunlight Induced Degradation of Fluoroquinolones in Wastewater Effluent: Photoproducts Identification and Toxicity, *Chemosphere*,**134**:313–318(2015).

[15] Xiang Y., Xu Z., Wei Y., Zhou Y., Yang X., Yang Y., Jian Y., Zhang J., Luoa L., Zhou Z., Carbon-based Materials as Adsorbent for Antibiotics Removal: Mechanisms and Influencing Factors, *Journal of Environmental Management*, **237**:128–138(2019).

[16] Huang B., Liu Y., Li B., Liu S., Zeng G., Zeng Z., Wang X., Ning Q., Zheng B., Yang C., Effect of Cu(II) Ions on the Enhancement of Tetracycline Adsorption by Fe_3O_4@SiO_2-Chitosan/Graphene Oxide Nanocomposite, *Carbohydr. Polym.*, **157**:576–585(2017).

[17] Huang L., Shi C., Zhang B., Niu S., Gao B., Characterization of Activated Carbon Fiber by Microwave Heating and the Adsorption of Tetracycline Antibiotics, *Separ. Sci. Technol.*, **48**: 1356–1363(2013).

[18] Ahmad K.S., Evaluating the Adsorption Potential of Alachlor and Its Subsequent Removal from Soils via Activated Carbon, *Soil and Sediment Contamination*, **27(4)**:249-266(2018).

[19] Ahmad K.S., Arachis Hypogaea Derived Activated Carbon Steered Remediation of Benzimidazole Based Fungicide Adsorbed Soils, *Chemistry and Ecology*, **35(6)**: 576-591(2019).

[20] Ahmad K.S., Adsorption Removal of Endosulfan through Saccharum Officinarum Derived Activated Carbon from Selected Soils, *J. Cent. South Univ.*, **26**:146−157 (2019).

[21] Ba S., Ennaciri K., Yaacoubi A., Alagui A., Bacaoui A., Activated Carbon from Olive Wastes as an Adsorbent for Chromium Ions Removal, *Iran. J. Chem. Chem. Eng. (IJCCE)*, **37(6)**: 107-123.

[22] Mandanipour V.., Sadeghi Maleki S.R., Pasandideh Nadamani M., Eparation of Adsorbents Containing CdS Quantum Dots from the Orange Peel for the Sewage Treatment, *Iran. J. Chem. Chem. Eng. (IJCCE)*, **40(3)**: 704-714 (2021).

[23] Yu F., Sun S., Han S., Zheng J., Ma J., Adsorption Removal of Ciprofloxacin by Multi-walled Carbon Nanotubes with Different Oxygen Contents from Aqueous Solutions, *Chemical Engineering Journal*, **285**:588–595(2016).

[24] Fakhri A., Adami S., Adsorption and Thermodynamic Study of Cephalosporins Antibiotics from Aqueous Solution onto MgO Nanoparticles, *J. Taiwan Inst. Chem. Eng.*, **45**:1001–1006 (2014).

[25] Wu H., Xie H., He G., Guan Y., Zhang Y., Effects of the pH and Anions on the Adsorption of Tetracycline on Iron-Montmorillonite, *Appl. Clay Sci.*,**119**:161–169 (2016).

[26] Erşan M., Bağda E., Bağda E., Investigation of Kinetic and Thermodynamic Characteristics of Removal of Tetracycline with Sponge Like, Tannin Based Cryogels, *Colloids Surfaces B Biointerfaces*, **104**:75–82(2013).

[27]Yang W., Zheng F., Lu Y., Xue X., Li N., Adsorption Interaction of Tetracyclines with Porous Synthetic Resins, *Ind. Eng. Chem. Res.*, **50**:3892–13898(2016).

[28] Hajmohammadi H., Jafari A.H.,Eskandari Nasab M. Adsorption of Scandium and Yttrium from Aqueous Solutions by Purolite C100Na Resin: Equilibrium and Kinetic Modeling. *Iran. J. Chem. Chem. Eng. (IJCCE)*, **40(4)**:1132-1147(2021).

[29] Hana H., Rafiq M.K., XuaT.Z., Mašekb R.O., Lia X.A., Critical Review of Clay-Based Composites with Enhanced Adsorption Performance for Metal and Organic Pollutants, *Journal of Hazardous Materials*,**369**:780–796(2018).

[30] Puri C., Sumana G., Highly Effective Adsorption of Crystal Violet Dye from Contaminated Water using Graphene Oxide Intercalated Montmorillonite Nanocomposite, *Appl. Clay Sci.*, **166**:102-112(2018).

[31] Uddin M.K., A Review on the Adsorption of Heavy Metals by Clay Minerals, with Special Focus on the Past Decade, *Chem. Eng. J.*, **308**:438–462(2016).

[32] Farajfaed S., Sharifian S., Asasian-Kolur N., Sillanpaa M., Granular Silica Pillared Clay for Levofloxacin and Gemifloxacin Adsorption from Aqueous Systems, *Journal of Environmental Chemical Engineering*, **9(106306)**: 1-16 (2021).

[33] Kalhori E.M., Al-Musawi T.J., Ghahramani E., Kazemian H., Zarrabi, M., Enhancement of the Adsorption Capacity of the Light-Weight Expanded Clay Aggregate Surface for the Metronidazole Antibiotic by Coating with MgO Nanoparticles: Studies on the Kinetic, Isotherm, and Effects of Environmental Parameters, *Chemosphere*, **175**: 8-20 (2017).

[34] Antonelli R., Martins F.R., Malpass G.R.P., Silva M.G.C., Vieira M.G.A., Ofloxacin Adsorption by Calcined Verde-lodo Bentonite Clay: Batch and Fixed Bed System Evaluation, *Journal of Molecular Liquids*,**315(113718)**:1-13(2020).

[35] Antonelli R., Malpass G.R.P., Silva M.G.C., Vieira M.G.A., Adsorption of Ciprofloxacin onto Thermally Modified Bentonite Clay: Experimental Design, Characterization, and Adsorbent Regeneration, *Journal of Environmental Chemical Engineering*, **8(104553):**1-12(2020).

[36] Duarte J.L.S., Solano A.M.S., Arguelho M.L.P.M., Tonholo J., Martínez-Huitle C.A., Zanta C.L.S., Evaluation of Treatment of Effluents Contaminated with Rifampicin by Fenton, Electrochemical and Associated Processes, *J. Water Process Eng.*, **22**: 250–257(2018).

[37] Henrique D.C., Quintelaa D.U., Idea A.H., Ertob A., Duartea J.L.S., Meilia L., Calcined, Mytella Falcata Shells as Alternative Adsorbent for Efficient Removal of Rifampicin Antibiotic from Aqueous Solutions, *Journal of Environmental Chemical Engineering*,**8**:103782(2020).

[38] Belaissa Y., Saib F., Trari M, Removal of Amoxicillin in Aqueous Solutions by a Chemical Activated Carbons Derived from Jujube Nuts: Adsorption Behaviors, Kinetic and Thermodynamic Studies, *Reac. Kinet. Mech. Cat.* (2022).

[39] Jawad A.H., Abdulhameed A.S., Mesoporous Iraqi Red Kaolin Clay as an Efficient Adsorbent for Methylene Blue Dye: Adsorption Kinetic, Isotherm and Mechanism Study, *Surfaces and Interfaces*, **18**: 1-7(2020).

[40] Yavuz Ö., Saka C., Surface Modification with Cold Plasma Application on Kaolin and its Effects on the Adsorption of Methylene Blue, *Appl. Clay Sci.*, **85**: 96–102(2013).

[41] Mouni L., Belkhiri L., Bollinger J.C., Bouzaza A., Assadi A., Tirri A., Remini H., Removal of Methylene Blue from Aqueous Solutions by Adsorption on Kaolin: Kinetic and Equilibrium Studies, *Appl. Clay Sci.*, **153**: 38–45 (2018).

[42] Xing S., Zhao M., Ma Z., Removal of Heavy Metal Ions from Aqueous Solution using Red Loess as an Adsorbent, *Journal of Environmental Sciences*, **23(9)**:1497–1502(2011).

[43] Conceiçãoa F.T., Silvaa M.S.G., Menegário A.A., Antunes M.L.P., Navarroa G.R.B., Fernandes A.M., Dorea C., Moruzzi R.B., Precipitation as the Main Mechanism for Cd(II), Pb(II) and Zn(II) Removal from Aqueous Solutions using Natural and Activated Forms of Red Mud, *Environmental Advances*,**4(100056)**: 1-10(2021).

[44] Cai W.L., Weng X.L., Chen Z.L., Highly Efficient Removal of Antibiotic Rifampicin from Aqueous Solution using Green Synthesis of Recyclable Nano-Fe_3O_4, *Environ. Pollut.*, **247**: 839-846(2019).

[45] Dalvand A., Nabizadeh R., Ganjali M.R., Khoobi M., Nazmara, S., Mahvi, A.H., Modeling of Reactive Blue 19 Azo Dye Removal from Colored Textile Wastewater using L-Arginine-Functionalized Fe_3O_4 Nanoparticles: Optimization, Reusability, Kinetic and Equilibrium Studies, *Journal of Magnetism and Magnetic Materials*, **404**:179–189 (2016).

[46] Wang Z., Wang G., Li W., Cui Z., Wu J., Akpinar I., Yu L., He G., Hu J., Loofah Activated Carbon with Hierarchical Structures for High-Efficiency Adsorption of Multi-Level Antibiotic Pollutants, *Applied Surface Science*, **550**:49313(2021).

[47] Sarma G.K., Gupta S.S., Bhattacharyya K.G., SN Removal of Hazardous Basic Dyes from Aqueous Solution by Adsorption onto Kaolinite and Acid-Treated Kaolinite: Kinetics, Isotherm and Mechanistic Study, *Applied Sciences*, **1(211)**: 1-15 (2019).

[48] Nandi B.K., Goswami A., Purkait M.K., Adsorption Characteristics of Brilliant Green Dye on Kaolin, *J. Hazard. Mater.*, **161(1)**:387–395(2009).

[49] Li X., Ji M., Nghiem L.D., Zhao Y., Liua D., Yang Y., Wang Q., Trinh Q.T., Vo D.N., Phame V.Q., Tran N.H., A Novel Red Mud Adsorbent for Phosphorus and Diclofenac Removal from Wastewater, *Journal of MolecularLiquids*,**303**:112286(2020).

[50] Li Y., Huang H., Xu Z., Ma H., Guo Y., Mechanism Study on Manganese(II) Removal from Acid Mine Wastewater using Red Mud and its Application to a Lab-Scale Column, *Journal of Cleaner Prod.*, **253**:1-12(2020).

[51] Pinto P.S., Lanza G.D., Souza M.N., Ardisson J.D., Lago R.M., Surface Restructuring of Red Mud to Produce FeOx(OH)y Sites and Mesopores for the Efficient Complexation /Adsorption of β- Lactam Antibiotics, *Environ. Sci. Pollut. Res.*, **25**: 6762–6771(2018).

[52] Deihimi N., Irannajad M., Rezai B., Characterization Studies of Red Mud Modification Processes as Adsorbent for Enhancing Ferricyanide Removal, *J. Environ. Manag*, **206**:266-275(2018).

[53] Liu X., Zhang N., Sun H., Zhang J., Li L., Structural Investigation Relating to the Cementitious Activity of Bauxite Residue-Red Mud, *Cement Concr. Res.*, **41**:847-853(2011).

[54] Khan M., N., Sarwar A., Determination of Points of Zero Charge of Natural and Treated Adsorbentes, *Surface Review and Letters*, **14(3)**:461–469(2007).

[54] Fadhil A.B., Saeed H.N., Saeed L.I., Polyethylene Terephthalate Waste-Derived Activated Carbon for Adsorptive Desulfurization of Dibenzothiophene from Model Gasoline: Kinetics and Isotherms Evaluation, *Asia-Pac. J. Chem. Eng.*, **16(2)**:1-13 (2020).

[55]Hussein, A.A., Fadhil, A.B., Kinetics and Isothermal Evaluations of Adsorptive Desulfurization of Dibenzothiophene Over Mixed Bio-Wastes Derived Activated Carbon, *Energy Sources, Part A: Recovery, Utilization, and Environmental Effects*, 1-21(2021).

[56] Khan, M.I., Adsorption of Methylene Blue onto Natural Saudi Red Clay: Isotherms, Kinetics and Thermodynamic Studies, M*ater. Res. Express*,**7**:1-14(2020).

[57] Rajaei G.E., Aghaie H., Zare K., Aghaie M., Adsorption of Cu(II) and Zn(II) Ions from Aqueous Solutions onto Fine Powder of Typha latifolia L. Root: Kinetics and Isotherm Studies, *Research on Chemical Intermediates*, **39**:3579–3594 (2013).

[58] Rajaei,G.E., Khalili-Arjaghi, S., Fataei,E.,Sajjadi, N., Kashefi-Alasl,M. Fabrication and Characterization of Polymer-Based Nanocomposite Membrane Modified by Magnetite Nanoparticles for Cd^{2+} and Pb^{2+} Removal from Aqueous Solutions, *Comptes Rendus. Chimie*., **23(9-10)**: 563-574(2020).

[59] Rezaei-Aghdam E., Shamel A., Khodadadi-Moghaddam M., Rajaei G.E., Mohajeri S., Synthesis of TiO_2 and ZnO Nanoparticles and CTAB-Stabilized Fe3O4 Nanocomposite: Kinetics and Thermodynamics of Adsorption, *Research on Chemical Intermediates*, **47(4)**:1759–1774 (2021).

[60] Khalili Arjaghi Sh., Ebrahimzadeh Rajaei Gh., Sajjadi N., Kashefi Alasl, M. Fataei E, Removal of Mercury and Arsenic Metal Pollutants from Water Using Iron Oxide Nanoparticles Synthesized from Lichen Sinensis Ramalina Extract, *Journal of Health*, **11(3)**: 397-408(2020).

[61] Xu, Q., Owens, G., Chen, Z., Adsorption and Catalytic Reduction of Rifampicin in Wastewaters Using Hybrid rGO@Fe/Pd Nanoparticles, *Journal of Cleaner Production*, **264(121617)**:1-10(2020).

[62] Kais, H., Mezenner, N.Y., Trari, M., Biosorption of Rifampicin from Wastewater using Cocoa Shells Product, *Separation Science and Technology*, **l55(11)**:1984-1993(2020).